Int. J. Heat Mass Transfer. Vol. 11, pp. 837–853. Pergamon Press 1968. Printed in Great Britain

UNSTEADY HEAT TRANSFER IN DUCTS WITH TIME-VARYING INLET TEMPERATURE AND PARTICIPATING WALLS

E. M. SPARROW and F. N. DE FARIAS

Coordenação dos Programas Pós-Graduados de Engenharia, Universidade do Brasil, Rio de Janeiro, Brasil

(*Received* 10 *April* 1967 *and in revised form* 2 *November* 1967)

Abstract—An analysis is made of unsteady laminar heat transfer in a duct with periodically varying inlet temperature and time- and space-dependent wall temperature. The wall temperature variation is not specified in advance, but rather, is dynamically determined by a balance of the heat-transfer rate and the energy storage. In the analytical formulation, the commonly used quasi-steady assumption is lifted in favor of the local application of the energy equation, the solution of which leads to an eigenvalue problem in which the eigenvalues are complex (real and imaginary parts). The series expansion properties of the corresponding complex eigenfunctions, which are essential to the solution, are verified. Numerical results are obtained for the time and space dependence of the wall and bulk temperatures and of the Nusselt number. These results identify conditions under which the wall temperature variations are negligible and the instantaneous Nusselt number is virtually time-independent. In addition, numerical information on the overall performance of the duct as a heat exchanger is provided by means of the ratio of the outgoing to the incoming energy flux. It is shown that for a wide range of operating conditions, the overall performance can be described by a single curve. For comparison purposes, results for the overall performance are also derived using the quasi-steady model. Quasi-steady results are evaluated for both spatially uniform and spatially varying heat-transfer coefficients. It was found that, for a range of operating conditions, the quasi-steady model is able to give accurate performance predictions, especially where it is used in conjunction with spatially varying heat-transfer coefficients.

NOMENCLATURE

a^*, heat capacity ratio, $\rho c_p L/(\rho c)_w \ell$;
b^*, parameter, $\omega L(\rho c)_w \ell/k$;
c, specific heat;
c_p, specific heat at constant pressure;
E, convected energy flux, equations (37) and (38);
h, heat-transfer coefficient, $q/(T_b - T_w)$;
k, thermal conductivity;
L, half-spacing between plates;
ℓ, half-thickness of wall;
Nu, Nusselt number, hL/k;
Pe, Péclet number, UL/α;
q, local heat flux/time-area;
T, fluid temperature;
T_b, bulk temperature;
T_0, cycle mean temperature;
T_w, wall temperature;
t, time;
U, mean velocity;
u, axial velocity;
x, axial coordinate;
y, transverse coordinate.

Greek symbols

α, thermal diffusivity, $k/\rho c_p$;
γ, real part of λ;
ΔT_0, amplitude of temperature variation;
δ, imaginary part of λ;
η, dimensionless coordinate, y/L;
θ, dimensionless temperature, $(T - T_0)/\Delta T_0$;
λ, eigenvalue;
ρ, density;
χ, dimensionless coordinate, $(x/L)/Pe$;
ω, circular frequency.

Subscripts

w, wall properties;
Fluid properties are unsubscripted.

INTRODUCTION

THE STUDY of unsteady forced convection heat transfer in tubes and ducts has been stimulated by heat exchanger applications. Processes such as start-up, shut-down, power surge, pump failure, etc. have motivated investigation of the thermal response of internal flows to step changes in thermal or hydrodynamic conditions. The periodic thermal response of duct flows to imposed cyclic variations has also been investigated, the motivation being provided by devices of the regenerative type through which hot and cold fluids pass in succession.

In analyzing thermal transients in internal flows, it is common to assume that quasi-steady conditions prevail [1, 2]; that is, that at each and every instant of time, the fluid experiences an instantaneous steady state. From the standpoint of practical computations, the quasi-steady assumption is equivalent to the instantaneous application of steady-state heat-transfer coefficients to the transient process. Although such a procedure is defensible for turbulent flows, its validity in the laminar case is open to question.

As a consequence of the aforementioned reservation, several analytical studies of transient laminar heat transfer in tubes and ducts have been performed wherein the quasi-steady assumption is lifted. Important contributions have been made by Perlmutter and Siegel ([3, 4] are representative of a series of papers) and by Hudson and Bankoff [5]. These authors have dealt with cases wherein the thermal conditions at the wall are prescribed (e.g. specified timewise variations of wall temperature, wall heat flux, or internal heat generation) and the inlet temperature of the fluid is steady.

In certain classes of problems, the temporal and spacial variations of the thermal conditions at the wall are generally unknown *a priori*; instead, they are determined by the dynamic interaction between the wall and the fluid. Moreover, the transient may be imposed by timewise variations of the fluid temperature at the inlet. The aforementioned characteristics are typified by the regenerative heat exchanger.

The present investigation is concerned with transient laminar heat transfer in a duct wherein the thermal conditions at the wall are determined by the dynamics of the problem and the inlet temperature is periodically varying. The quasi-steady assumption for the heat-transfer coefficient is set aside, and instead, energy conservation (including storage) is applied at all points throughout the fluid.

Specific consideration is given to laminar flow in a parallel plate channel. The fluid inlet temperature is assumed to vary periodically in a sinusoidal manner with an arbitrary frequency, thereby facilitating a Fourier series synthesis to accommodate other periodic variations. The velocity of the flow is unchanging with time. The mid-plane of each channel wall is regarded as insulated, as would be the case if the channel under study were a member of an ensemble of similar channels. The temporal and spacial variations of the wall temperature result from the corresponding variations of the heat-transfer rate at the wall, interacting with the wall heat capacity. In turn, the wall heat-transfer rate itself depends on the wall temperature. It is clear that there is a strong mutual influence between thermal processes in the wall and in the fluid, such a mutual influence being absent when the thermal state is prescribed at the wall.

A periodic solution of the just-described problem is sought, and this leads to an eigenvalue problem wherein the eigenvalues are complex (real and imaginary parts). The corresponding eigenfunctions are also complex, and these are summed in accordance with the linearity of the energy equation. The coefficients of the resulting series are found by employing the specified temperature condition at the duct inlet. In this latter connection, it may be observed that the mathematical system encountered here does not belong to the Sturm–Liouville family and therefore, the well-established orthogonality and series expansion characteristics of Sturm–Liouville eigenfunctions are inapplicable. To establish the validity of the present solution, the orthogonality and expansion properties of the

participating series were investigated and verified.

The numerical evaluation of the solution provides a variety of results of engineering interest. These include local quantities such as the wall temperature and the bulk temperature, which vary with time and with axial position to an extent that depends on the physical parameters of the problem. The aforementioned temperatures used in conjunction with the local instantaneous wall heat flux permit the evaluation of a local instantaneous heat-transfer coefficient, which can then be compared with the quasi-steady value. In addition, results for the overall performance of the channel as a heat exchanger are presented in terms of the energy carried across the exit cross section relative to that carried across the entrance section.

In connection with the aforementioned overall performance, it was deemed worthwhile to compare the results based on the energy equation solutions with those based on the quasi-steady model. For this purpose, the quasi-steady model was applied in two ways: (1) using the fully-developed heat-transfer coefficient; (2) using local entrance region heat-transfer coefficients. These comparisons provide insights into the parameter ranges in which the quasi-steady model provides accurate predictions of overall performance.

From a survey of the literature, it appears that the problem investigated by Kardas [6] comes closest to the physical situation treated here. However, Kardas employed the quasi-steady model (and also neglected the fluid heat capacity), presumably with the turbulent case in mind. As outlined above, the present investigation sets aside the quasi-steady assumption, and instead, deals directly with the energy equation applied at each point in the flow.

As a final introductory remark, it is interesting to observe that laminar flow regenerators already exist in engineering practice, for instance [7]. The flow passages of the system described in the just-cited reference are flat rectangular ducts, closely resembling the parallel plate channel selected for study here.

ANALYSIS AND SOLUTION

Formulation of the problem

Consider a parallel plate channel whose bounding surfaces are separated by a distance $2L$ and whose walls are each of thickness 2ℓ. A steady laminar flow passes through the channel. The fluid entering the channel has a temperature which varies sinusoidally with time. Owing to the timewise variation of the fluid temperature, heat is alternately transferred from the fluid to the wall and from the wall to the fluid.

It is assumed that the mid-plane of each wall (parallel to the wall–fluid interface and displaced from it by a distance ℓ) is impermeable to heat. Such a condition would exist, for instance, if the channel under consideration were one of several in an ensemble. Alternatively, the same condition could be achieved if the walls had thickness ℓ and were insulated on their external surfaces. In either case, the walls are regarded as sufficiently thin and/or the thermal diffusivity sufficiently high so that the temperature variation across the thickness of the wall is negligible.† In view of this, the wall temperature remains as a function of time and of axial position.

Axial distances from the entrance section are measured by the coordinate x, while transverse distances are measured by y (the duct centerline corresponds to $y = 0$).

The starting point of the analysis is the unsteady energy equation for the fluid, specialized to the case wherein transverse velocities are negligible

$$\rho c_p\left(\frac{\partial T}{\partial t} + u\frac{\partial T}{\partial x}\right) = k\frac{\partial^2 T}{\partial y^2}. \tag{1}$$

Equation (1) has been written without the axial conduction term in recognition of the fact that low Péclet number flows (e.g. liquid metals) are

† Such a state of affairs exists when the diffusion time for the wall, approximately given by $\ell^2/(k/\rho c)_w$, is substantially smaller than the period of the timewise temperature variations.

typically not encountered in heat-transfer systems of the type being studied here.† Fluid property variations are also neglected.

Next, focusing attention on the wall and using the aforementioned postulate of a relatively short diffusion time, it is sufficient to make an energy balance on an element of thickness ℓ and axial extension dx. If q denotes the instantaneous rate of heat transfer per unit time and unit area, then one can write that

$$\ell(\rho c)_w \frac{\partial T_w}{\partial t} = q = -k\left(\frac{\partial T}{\partial y}\right)_{y=L} \tag{2}$$

where Fourier's law has also been used. The temperature at the interface between the fluid and the wall must be continuous, and consequently, $T(x, L, t) = T_w(x, t)$. With this, equation (2) becomes

$$\frac{\partial T}{\partial t} = -\frac{k}{\ell(\rho c)_w}\frac{\partial T}{\partial y} \quad \text{at} \quad y = L. \tag{2a}$$

It now remains to specify the thermal condition of the fluid at the entrance of the channel. The fluid temperature is assumed to be spacially uniform across the entrance section and to vary sinusoidally in time. For purposes of analysis, it is convenient to express the latter in complex exponential form, that is

$$T - T_0 = \Delta T_0 \, e^{i\omega t} \tag{3}$$

where T_0 is the cycle-mean temperature and ΔT_0 is the amplitude.

For present purposes, it is not necessary to state initial conditions (i.e. at $t = 0$) inasmuch as a periodic solution is being sought.

Solution

To simplify the computational aspects of the solution, it will now be assumed that $u = U$ (i.e. slug flow) where U is the mean velocity. This step is motivated solely by computational convenience and does not influence the essential nature of the results.

† For instance, regenerative heat exchangers generally operate with gas flows.

A periodic temperature solution of the following form is proposed

$$\theta = A \, e^{i\omega t} X(\chi) \, Y(\eta) \tag{4}$$

in which θ, χ, and η are dimensionless variables defined as

$$\theta = \frac{T - T_0}{\Delta T_0}, \qquad \eta = \frac{y}{L}, \qquad \chi = \frac{x/L}{Pe} \tag{5}$$

and Pe $(= UL/\alpha)$ is the Péclet number. Upon substituting the proposed solution into equation (1), the explicit forms of $X(\chi)$ and $Y(\eta)$ follow as

$$X = \exp\left[-\lambda^2\chi\right] \exp\left[-(L^2/\alpha)i\omega\chi\right], \qquad Y = \cos\lambda\eta \tag{6}$$

wherein the Y solution embodies the condition of thermal symmetry at the centerline of the channel (i.e. at $y = 0$).

The quantity λ is an eigenvalue, the numerical values of which are to be determined so that the condition (2a) is satisfied. The substitution of the solution (6) into equation (2a) yields

$$\lambda \tan\lambda = ib^* \tag{7}$$

where b^* is a parameter that includes wall and fluid properties and dimensions as well as the circular frequency ω of the imposed temperature variation, i.e.

$$b^* = \frac{\omega L(\rho c)_w \ell}{k}. \tag{8}$$

Typically, practical values of b^* are in excess of unity.

Equation (7) serves as a condition from which the eigenvalues can be determined. The novel aspect of equation (7), which sets it aside from conventionally encountered eigenvalue problems, is the appearance of the complex number i. Since b^* is a real number, it follows that λ must be complex. In recognition of this, it is natural to define

$$\lambda = \gamma + i\delta \tag{9}$$

and, upon substitution into equation (7), there follows after use of the identities $\cos i\delta = \cosh\delta$

and $\sin i\delta = i \sinh \delta$ and segregation of the real and imaginary parts

$$\frac{\gamma}{\tanh \delta} - \frac{\delta}{\tan \gamma} = b^* \tag{10a}$$

$$\gamma \tanh \delta + \delta \tan \gamma = b^*. \tag{10b}$$

Equations (10) constitute a pair of coupled transcendental equations, the simultaneous solution of which provides γ and δ.

For any given value of b^*, there are a sequence of (γ, δ) pairs which satisfy equations (10). Let these be arranged in ascending magnitude of γ (the difference between successive γ is approximately π) and labeled (γ_1, δ_1), (γ_2, δ_2), etc. The method and other aspects of the eigenvalue calculation will be discussed later.

In view of the linearity of the problem, a general solution for any given b^* value can be constructed by adding together the separate solutions corresponding to each λ_n; thus, from equations (4) and (6),

$$\theta = \sum_{n=1} A_n \exp\{i\omega[t - (L^2/\alpha)\chi]\} \times \exp[-\lambda_n^2 \chi] \cos \lambda_n \eta. \tag{11}$$

To complete the solution, it remains to evaluate the coefficients A_n and, at the same time, to satisfy the prescribed timewise temperature variation at the entrance cross section. By bringing together equations (3) and (11), and evaluating the latter at $\chi = 0$, one finds

$$1 = \sum_{n=1} A_n \cos \lambda_n \eta. \tag{12}$$

The foregoing equation, although deceptively simple in appearance, is decisively different from the series expansions encountered in conventional steady-state entrance region analyses. The fact that the λ_n are complex places the present eigenvalue problem outside the framework of the Sturm–Liouville theory, and therefore the well-established orthogonality and series expansion properties of the latter cannot be applied. It is therefore necessary to prove the validity of the expansion (12) by other means; this matter, as well as orthogonality, is treated in the next section.

For the present, let it be assumed that equation (12) is a valid expansion and that the $\cos \lambda_n \eta$ are orthogonal. Then, upon multiplying (12) by $\cos \lambda_m \eta$ and integrating over the range $\eta = 0$ to $\eta = 1$, there is obtained

$$A_n = 4 \sin \lambda_n / (2\lambda_n + \sin 2\lambda_n) \tag{13}$$

where A_n is a complex quantity because λ_n is complex.

Equations (11) and (13), taken together, constitute a solution for the time-dependent temperature field in the fluid when the timewise temperature at the inlet section is a complex exponential, equation (3). The temperature solution is, correspondingly, complex. In order to relate the results to reality, consideration must now be given to the real forms both of equation (3) and of the temperature solution. As far as the former is concerned, one may arbitrarily employ either $\sin \omega t$ or $\cos \omega t$. If the sine is selected, then the inlet condition becomes

$$T - T_0 = \Delta T_0 \sin \omega t, \qquad \text{at} \quad x = 0. \tag{14}$$

The corresponding temperature solution is derived by taking the imaginary part of equation (11), following substitution of A_n from (13). After considerable algebraic manipulation, there results

$$\theta = 4 \sum_{n=1} \exp[-(\gamma_n^2 - \delta_n^2)\chi] \times \{[\Phi_n(\eta) Z_n(\chi) - \varphi_n(\eta) \zeta_n(\chi)] \cos \omega t + [\Phi_n(\eta) \zeta_n(\chi) + \varphi_n(\eta) Z_n(\chi)] \sin \omega t\}. \tag{15}$$

The expressions for Φ, φ, Z, and ζ are rather lengthy and have therefore been relegated to the Appendix. If these functions and their subsidiary computational groupings are inspected, it is found that θ depends on two dimensionless parameters. One of these, b^*, has already been defined by equation (8). The second, a^*, is a ratio of heat capacities, that is

$$a^* = \frac{\rho c_p L}{(\rho c)_w \ell}. \tag{16}$$

It can be shown that the appearance of a^*

in the problem stems directly from the heat storage term in the energy equation for the fluid; that is, if the heat storage in the fluid were neglected, a^* would disappear as a parameter. In systems where the fluid is a gas and the wall is metallic, a^* is very much less than one.

Numerical evaluation of equation (15) yields the fluid temperature at any position (χ, η) in the channel for any time t. Moreover, by taking $\eta = 1$, the wall temperature is obtained. In addition, the bulk temperature, wall heat flux, heat-transfer coefficient, overall energy transport, etc., can all be determined with the aid of equation (15) and its integrated or differentiated forms. Expressions for these quantities will be discussed later.

Validity of the series expansion; orthogonality

To insure the validity of the just-derived temperature solution, it is necessary to demonstrate that equation (12) represents a valid expansion; that is, that unity can indeed be expanded in terms of $\cos \lambda_n \eta$, $0 \leqslant \eta < 1$, when λ_n is complex.

The demonstration begins by recalling that the set of eigenfunctions $\cos \lambda_n \eta$ are generated by the mathematical system

$$Y'' + \lambda^2 Y = 0, \qquad Y'(0) = 0, \qquad Y'(1) + ib^* Y(1) = 0 \tag{17}$$

where the primes represent derivatives and $0 \leqslant \eta < 1$. It is now fruitful to consider the related system

$$\hat{Y}'' + \Lambda \hat{Y} = -f(\eta) = -1 \tag{18a}$$

$$\hat{Y}'(0) = 0, \qquad \hat{Y}'(1) + ib^* \hat{Y}(1) = 0. \tag{18b}$$

The choice $f(\eta) = 1$ stems from the fact that it is the function unity for which a series representation is being sought. By making use of the development given by Friedman [8] pp. 213–232), $f(\eta)$ can be expressed in terms of the $\hat{Y}$ as follows

$$f(\eta) = \lim_{R \to \infty} \frac{1}{2\pi i} \oint \hat{Y}_\Lambda(\eta)\, d\Lambda \tag{19}$$

the integration being taken around the contour of a circle of radius R.

It remains to solve equations (18) for $\hat{Y}$ and then to introduce the solution into equation (19). In a straightforward manner, one finds

$$Y_\Lambda(\eta) = -\frac{1}{\Lambda} + \frac{ib^* \cos \Lambda^{\frac{1}{2}} \eta}{\Lambda \cos \Lambda^{\frac{1}{2}} (ib^* - \Lambda^{\frac{1}{2}} \tan \Lambda^{\frac{1}{2}})}. \tag{20}$$

Next, substituting into (19) and making use of the theorem of residues, one finds

$$1 = \sum_{n=1} a_n \cos \lambda_n \eta. \tag{21}$$

The λ_n correspond to the successive zeros of the denominator of the second term on the right of equation (20) and are, at the same time, the eigenvalues which stem from equation (7). The a_n are complex constants. Equation (21) validates the expansion (12).

The demonstration that the $\cos \lambda_n \eta$ are orthogonal is performed in the conventional manner (for instance, see Hildebrand [9]) and need not be detailed here.

THE QUASI-STEADY MODEL

In order to facilitate a later comparison of results, the problem will now be analyzed under the assumption that steady-state heat-transfer coefficients apply instantaneously, that is

$$q = h(T_b - T_w) \tag{22}$$

where q, T_b, and T_w are functions of time, but h is time independent. Normally, when this model is used, h is assumed to be a constant, independent of axial position. However, in the development that follows, h will be permitted to be a function of x.

In applying the quasi-steady model, cross sectional variations of the fluid temperature are not considered. Instead, one works with the bulk temperature, which is defined as

$$T_b = \int_0^L uT\, dy \Big/ \int_0^L u\, dy = \frac{1}{L} \int_0^L T\, dy \tag{23}$$

where the last form is appropriate to slug flow.

An energy balance for a control volume spanning the duct cross section is obtained by integrating equation (1) from $y = 0$ to $y = L$, thus

$$\rho c_p L\left(\frac{\partial T_b}{\partial t} + U\frac{\partial T_b}{\partial x}\right) = -q = -h(T_b - T_w) \quad (24)$$

where equations (22) and (23) have also been used. The energy balance on an element of the duct wall is expressed by equation (2), which, in light of (22), now becomes

$$\ell(\rho c)_w \frac{\partial T_w}{\partial t} = h(T_b - T_w). \quad (25)$$

Periodic solutions for T_b and T_w may be written as

$$\theta_b = e^{i\omega t} F(\chi), \theta_w = e^{i\omega t} G(\chi). \quad (26)$$

The F and G functions are readily derived by applying equations (24) and (25), from which follow

$$F = \exp\left[-b^{*2} I_1(\chi)\right] \exp\left\{-ib^*[a^*\chi + I_2(\chi)]\right\} \quad (27)$$

$$G = F\frac{Nu(Nu - ib^*)}{Nu^2 + b^{*2}} \quad (28)$$

where

$$\left.\begin{aligned} I_1(\chi) &= \int_0^\chi \frac{Nu}{Nu^2 + b^{*2}}\,d\chi, \\ I_2(\chi) &= \int_0^\chi \frac{Nu^2}{Nu^2 + b^{*2}}\,d\chi \end{aligned}\right\} \quad (29)$$

and Nu $(=hL/k)$ is the Nusselt number. When the entering fluid temperature is a sine function, that is, equation (14), the solutions for T_b and T_w become

$$\theta_b = \exp\left[-b^{*2} I_1(\chi)\right] \sin\left[\omega t - J(\chi)\right] \quad (30)$$

$$\theta_w = \exp\left[-b^{*2} I_1(\chi)\right] \frac{Nu}{Nu^2 + b^{*2}} \times \left\{Nu \sin\left[\omega t - J(\chi)\right] - b^* \cos\left[\omega t - J(\chi)\right]\right\} \quad (31)$$

in which

$$J(\chi) = b^*[a^*\chi + I_2(\chi)]. \quad (32)$$

Inspection of equation (31) suggests certain interesting relationships between the wall and bulk temperatures. When $b^* \ll Nu$, then T_w and T_b are very nearly in phase, and $|T_w - T_b|$ is small. On the other hand, when $b^* \gg Nu$, there is a phase difference of nearly 90 deg between T_w and T_b; moreover, the amplitude of the wall temperature variation is much smaller than that of the bulk temperature variation.

The solutions derived above, particularly equation (30), will be applied in the Results section.

RESULTS AND DISCUSSION

As an essential ingredient for the numerical evaluation of the results, it is necessary to know the eigenvalues $\lambda_n (= \gamma_n + i\delta_n)$, the real and imaginary parts of which satisfy equations (10). For computational convenience, it was found advantageous to replace equation (10a) by

$$2\gamma \sin 2\gamma = 2\delta \sinh 2\delta. \quad (33)$$

Numerical values of γ and δ were determined by a trial and error procedure making consecutive use of equations (33) and (10b).

The eigenvalues depend parametrically on the dimensionless grouping b^* defined by equation (8). The range of b^* from 1 to 100 was selected as a basis for numerical study, this range encompassing operating conditions in regenerative heat exchangers.† The specific b^* values for which eigenvalues were determined included 1, 2, 5, 10, 50 and 100. The corresponding eigenvalues are listed in Table 1. In general, it was found that eight or nine eigenvalues were sufficient to provide results of high accuracy for all of the cases investigated here. For some of the b^* included in Table 1 (i.e. the higher b^*), a substantially larger number of eigenvalues were available, and it was thought better to list these values rather than to discard them. For the lower b^* of the table, additional eigenvalues can be generated by successively adding π to γ and evaluating δ as $\tanh^{-1}[b^*/(n-1)\pi]$.

† For instance, for the system discussed in [7], b^* ranged from 10 to 30.

Table 1. Eigenvalues

$b^* = 1$		$b^* = 2$		$b^* = 5$		$b^* = 10$		$b^* = 50$		$b^* = 100$	
γ	δ	γ	δ	γ	δ	γ	δ	γ	δ	γ	δ
0·8000	0·5709	1·1736	0·5809	1·5024	0·3104	1·5547	0·1569	1·57016	0·0316	1·570641	0·0156
3·1764	0·3228	3·3106	0·6485	4·2112	0·9928	4·6491	0·4981	4·71047	0·0950	4·711904	0·0483
6·2873	0·1581	6·3005	0·3192	6·3893	0·7026	7·6349	0·9625	7·85072	0·1590	7·853190	0·0786
9·4260	0·1072	9·4299	0·2158	9·4696	0·5828	10·1288	1·3513	10·99088	0·2233	10·994458	0·1101
12·5668	0·0814	12·5680	0·1605	12·5822	0·4193	12·7244	1·0284	14·13088	0·2894	14·135718	0·1418
15·7080	0·0623	15·7087	0·1280	15·7154	0·3296	15·7578	0·7449	17·27059	0·3595	17·276959	0·1744
18·8496	0·0531	18·8501	0·1065	18·8536	0·2709	18·8725	0·5887	20·40997	0·4326	20·418188	0·2071
21·9912	0·0455	21·9914	0·0912	21·9937	0·2314	22·0039	0·4898	23·54882	0·5111	23·559438	0·2399
25·1328	0·0398	25·1329	0·0798	25·1344	0·2016	25·1407	0·4207	26·68690	0·5950	26·700592	0·2731
		28·2744	0·0709	28·2755	0·1768	28·2797	0·3682	29·82380	0·6872	29·841750	0·3075
				31·4160	0·1608	31·4197	0·3294	32·95879	0·7903	32·982874	0·3426
				34·5576	0·1447	34·5603	0·2979	36·09032	0·9107	36·123959	0·3782
						37·7014	0·2782	39·21532	1·0536	39·264996	0·4149
						40·8421	0·2516	42·32487	1·2374	42·405975	0·4526
								45·38896	1·4902	45·546871	0·4922
								48·27723	1·8327	48·687704	0·5319
								50·83724	1·9341	51·828420	0·5740
								53·61037	1·6302	54·969012	0·6178
								56·64442	1·3774	58·109418	0·6642
								59·74631	1·2068	61·249636	0·7129
								62·86906	1·0839	64·389560	0·7653
								66·00010	0·9898	67·529149	0·8202
										70·668257	0·8798
										73·806643	0·9459
										76·944054	1·0185

With the eigenvalues thus available, all quantities of engineering interest can be evaluated from equation (15) and equations derived therefrom. Local quantities for which numerical results are to be given include the wall temperature, the bulk temperature, and the local Nusselt number. The overall performance of the duct-fluid system is represented in terms of the energy carried out of the duct exit section, relative to that carried into the duct through its entrance section. The just-mentioned energy outflow was evaluated not only by applying equation (15), but also from the quasi-steady solution (30), both with Nu = constant and $Nu = Nu(x)$.

Wall temperature

The spacial and temporal distributions of the wall temperature follow by specializing equation (15) to $\eta = 1$. Numerical results depend upon the parameters a^* and b^*. For the former, values of 0, 0·001, and 0·01 were employed,† yielding essentially identical wall temperature results within the scale of the forthcoming graphical presentation. For b^*, space limitations preclude use of all the values available (i.e. Table 1), and 1, 2, 10 and 100 were selected as providing representative information.

The wall temperature results thus obtained are presented in Figs. 1 and 2, the first of which corresponds to $b^* = 1$ and 2, while the second is for $b^* = 10$ and 100. Figure 1 contains separate graphs for the respective b^* values, while in Fig. 2 the results for $b^* = 10$ and 100 appear on a single graph. In all cases, the dimensionless wall temperature $(T_w - T_0)/\Delta T_0$ is plotted as a function of time at various axial stations χ. The abscissa spans one complete cycle and, since the solution is periodic, this is sufficient to specify the results at any time. At $\chi = 0$, i.e. at the entrance section, the wall temperature is identical to that of the entering fluid,‡ so that

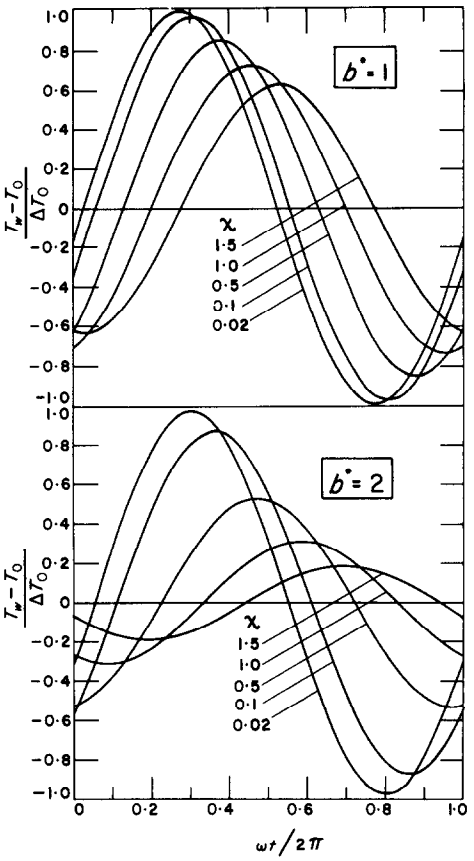

FIG. 1. Wall temperature results, $b^* = 1$ and 2.

$$(T_w - T_0)/\Delta T_0 = \sin \omega t. \qquad (34)$$

A curve corresponding to equation (34) is shown in Fig. 2.

An overall inspection of the figures reveals several significant trends. First of all, considering a given physical situation characterized by a fixed b^*, it is seen that the amplitude of the timewise temperature variation diminishes monotonically with increasing axial distance from the duct entrance. Moreover, the maxima (and minima) of the successive curves are displaced in time, indicating an increasing phase lag as the downstream distance increases. Both of the aforementioned trends are connected with the heat capacity of the wall. The effect of the

† An estimate, based on incomplete information, indicates an a^* value on the order of 0·0005 for the system of [7].

‡ This is because the heat-transfer coefficient is infinite at $\chi = 0$.

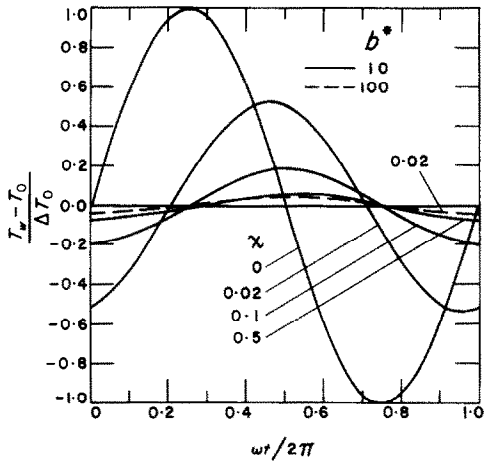

FIG. 2. Wall temperature results, $b^* = 10$ and 100.

wall is to dampen the amplitude of the timewise fluid temperature oscillations, such attenuation, in turn, being reflected in a dampening of the wall temperature oscillations. This process proceeds progressively along the duct.

It is also interesting to note that the phase lag is very little influenced by the time x/U required for the fluid to flow from $\chi = 0$ to $\chi = \chi$. In this connection, it is easily verified that the dimensionless time $(x/U)\omega$ is equal to $\chi a^* b^*$. Thus, for instance, when $\chi = 0{\cdot}1$, $a^* = 0{\cdot}001$ and $b^* = 10$, the foregoing quantity is 0·001. This is indeed small compared with the phase lag, evidenced in Fig. 2,† between $\chi = 0$ and $\chi = 0{\cdot}1$. The contribution of the fluid heat capacity to the phase lag is governed directly by the magnitude of $(x/U)\omega$, which is very small for all the cases depicted in Figs. 1 and 2. Therefore, it follows that the phase lags evidenced in these figures are attributable to the effects of the wall heat capacity.

Further inspection of Figs. 1 and 2 shows that increasing values of the parameter b^* have a decisive influence both in diminishing the amplitude of the timewise temperature variation and in increasing the phase lag. Indeed, for $b^* = 100$, the amplitude is already so small at $\chi = 0{\cdot}02$ that curves for larger downstream distances essentially coincide with a horizontal line, within the scale of the figure. Thus, for all x locations except those very close to the duct inlet, the $b^* = 100$ case (and, for that matter, all larger b^*) may be regarded as having steady and uniform wall temperature, wherein $T_w = T_0$. Such a model may also be useful, as a first approximation, for b^* between 10 and 100.

If, for purposes of discussion, the magnitude of b^* is regarded as a measure of the wall heat capacity, then the aforementioned trends immediately appear reasonable. That is, a wall with small heat capacity experiences relatively little amplitude attenuation and phase lag, while a wall with high heat capacity experiences large attenuation and lag. An equally satisfactory intuitive argument can be made by regarding b^* as a measure of the frequency of the imposed temperature oscillation.

Bulk temperature

An analytical representation for the bulk temperature may be derived by integrating the temperature solution (15) over the cross section in accordance with equation (23). The resulting expression is quite lengthy and since it, in itself, offers few insights, it is omitted in the interests of a more concise presentation.

Numerical evaluation of the temporal and spacial variations of the bulk temperature has been carried out for the same values of the parameters a^* and b^* as were employed for the wall temperature. The results thus obtained are presented in Figs. 3 and 4, the structure of which is similar to that of the foregoing Figs. 1 and 2. However, whereas the T_w results for $b^* = 10$ and 100 were conveniently presented on a single graph (Fig. 2), the T_b results for these b^* values are expeditiously shown on separate graphs (Fig. 4). Within the scale of the figures, the bulk temperature results for $b^* = 1$, 2, and 10 are the same for $a^* = 0$, 0·001 and 0·01. For $b^* = 100$, separate curves are shown, when necessary, for different a^* values.

†The phase lag read from the figure must be multiplied by 2π before comparing with $(x/U)\omega$.

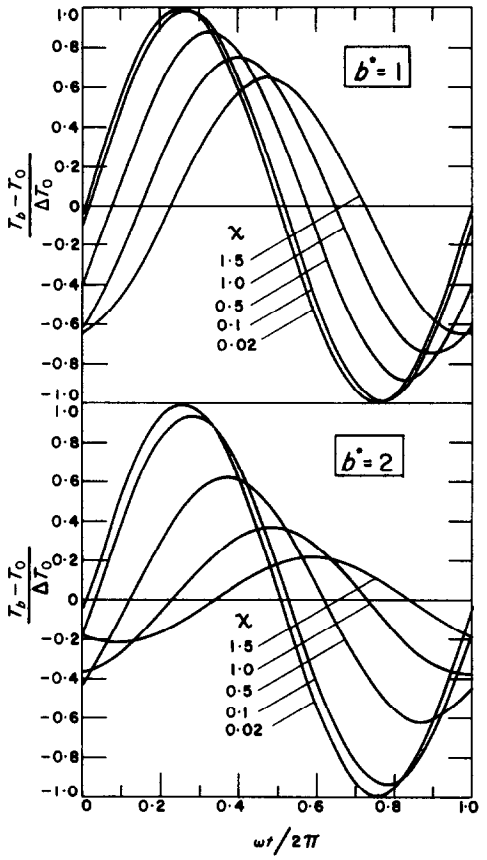

FIG. 3. Bulk temperature results, $b^* = 1$ and 2.

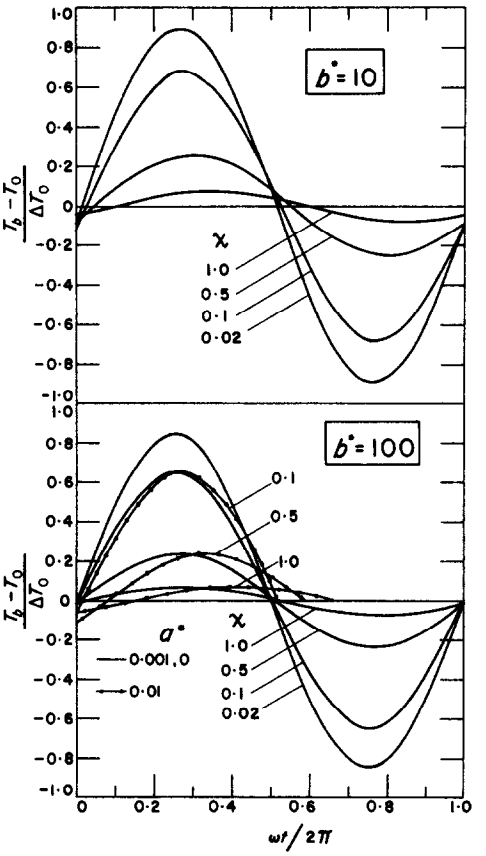

FIG. 4. Bulk temperature results, $b^* = 10$ and 100.

The bulk temperature results display some trends similar to those already enumerated for the wall temperature, but there are some significant differences. While, as before, amplitude attenuation and phase lag are accentuated with increasing downstream distance, the influence of b^* on these trends is quite different from that observed in the case of the wall temperature. At lower b^* values, say $b^* = 1$, the amplitude attenuation and phase shift displayed by the bulk temperature are nearly identical to those of the wall temperature. However, at higher b^*, the attenuation of the bulk temperature amplitude with χ is much less rapid than for the wall temperature (compare Figs. 2 and 4). In general, the dampening of the timewise temperature variations with increasing b^*, which was so overwhelming at the wall, is much more moderate for the bulk.

These findings are readily interpreted by regarding b^* as a measure of the wall heat capacity. When the wall heat capacity is very small, the bulk and wall temperatures are only slightly different. On the other hand, when the wall heat capacity is large, the wall temperature is constrained to a nearly constant value, while the fluid temperature is free to vary.

From further consideration of Figs. 3 and 4, it is seen that while the phase lag at smaller b^* values is large and increases markedly with increasing downstream distance, the same is not true at large b^* values. Indeed, for the latter,

the phase lag is substantially smaller and of a different character, as witnessed by the influence of the parameter a^*.

This behavior can be made plausible by noting that the phase lag experienced by the bulk temperature is the result of two factors: (1) the timewise variation of the wall temperature, (2) the heat capacity of the fluid itself. At small b^*, the wall temperature variation is relatively large and is effective in "driving" the fluid temperature variation. Moreover, since the importance of the fluid heat capacity is related to the magnitude of the quantity $(x/U)\omega = \chi a^* b^*$, it is evident that this effect is small at small b^*. When b^* is large, the wall temperature is essentially constant and therefore, it does not impress a phase lag on the bulk temperature variation. On the other hand, the fluid heat capacity may become significant if a^* is large enough, as follows from the fact that $(x/U)\omega = 1$ when $a^* = 0{\cdot}01$, $b^* = 100$, and $\chi = 1$.

Local heat-transfer coefficient

With a view toward assessing the quasi-steady model, the results of the present investigation will now be employed to evaluate a local heat-transfer coefficient h. In light of the aforementioned motivation, it is logical to define h as it is used in quasi-steady type analyses, that is

$$h = \frac{q}{T_b - T_w}. \tag{35}$$

The local instantaneous heat flux is evaluated by applying Fourier's Law

$$q = -k(\partial T/\partial y)_{y=L} \tag{36}$$

to the temperature solution (15). The temperatures T_w and T_b are found by specializing equation (15) in the manner already described. The resulting expression for h is rather lengthy and is, consequently, omitted.

Heat-transfer coefficients, numerically evaluated from the just-discussed equation, are presented in Figs. 5 and 6 in the form of a Nusselt number $Nu = hL/k$. Each of these

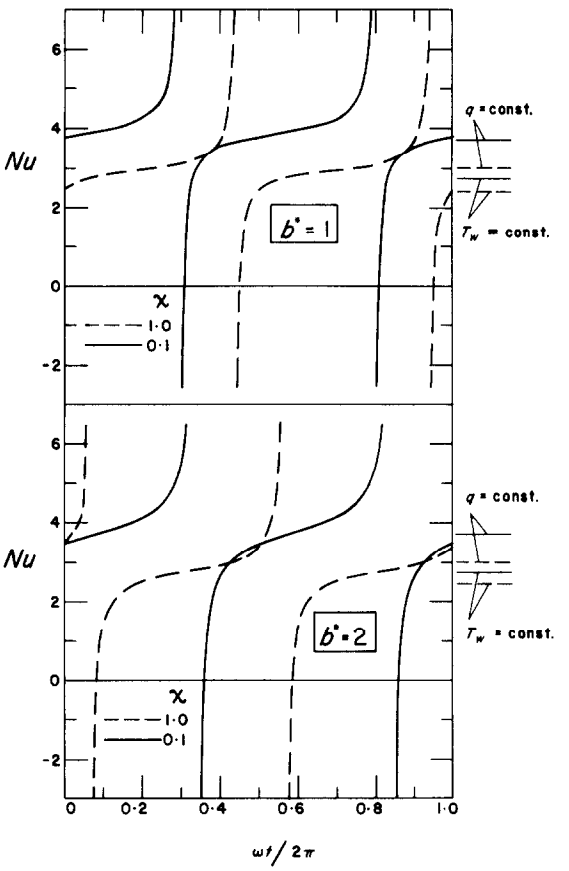

FIG. 5. Local Nusselt number results, $b^* = 1$ and 2.

figures is subdivided into upper and lower portions, each portion corresponding to a specific value of b^*. Figure 5 is for $b^* = 1$ and 2, and Fig. 6 is for $b^* = 10$ and 100. In each figure, Nu is plotted as a function of time for one cycle. Results are given for $\chi = 0{\cdot}1$ and $1{\cdot}0$, other χ values having been omitted to preserve clarity. For all cases shown in the figures, $a^* = 0{\cdot}001$.

Inspection of the figures reveals that the heat-transfer coefficient, as defined above, experiences discontinuities, soaring to plus infinity and then returning from minus infinity. These excursions occur when the wall and bulk temperatures are equal, but the heat flux is not zero. The Nusselt number is positive during most of the cycle, indicating that the heat flow is from the wall to the fluid when $T_w > T_b$ (or

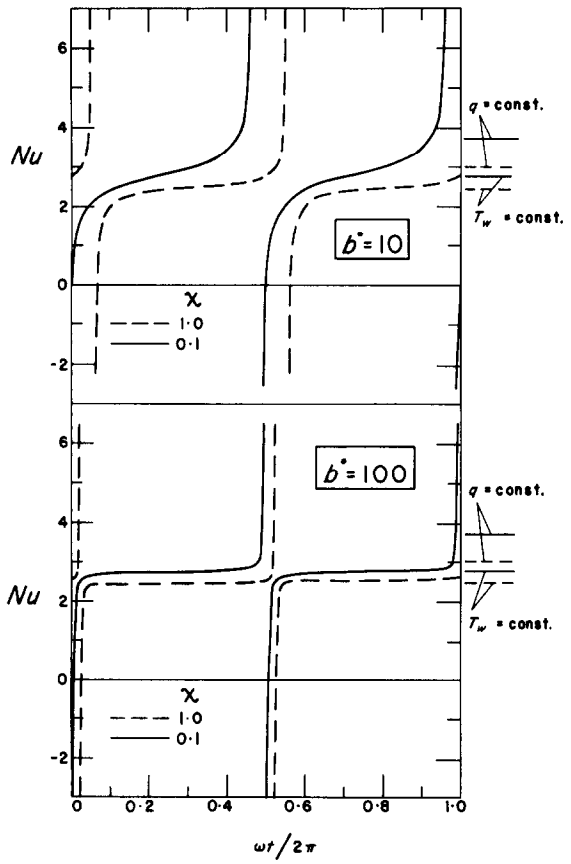

FIG. 6. Local Nusselt number results, $b^* = 10$ and 100.

vice versa). However, there is a short period during each cycle when the Nusselt number is negative, such that heat flows from the wall to the fluid when $T_w < T_b$.

In a presentation such as Figs. 5 and 6, the quasi-steady condition for each case would be represented by a horizontal line. It thus appears that quasi-steady operation is approached at large values of b^*. Also, in all cases, quasi-steady conditions are more closely approximated at large downstream distances than at locations very near the duct inlet.

It can be reasoned that, if the fluid heat capacity is neglected, the local instantaneous heat-transfer coefficient will become time-independent in both limits as b^* approaches zero and infinity. It therefore follows that the greatest deviations occur in the intermediate range. This explains why, among the Nusselt number results of Fig. 5, those for $b^* = 1$ are closer to quasi-steady than are those for $b^* = 2$.

In the right-hand margins of both Figs. 5 and 6 are shown horizontal lines representing local steady-state Nusselt numbers for the boundary conditions of uniform wall temperature (T_w = const.) and uniform heat flux (q = const.). In all cases wherein quasi-steady operation is approached, the horizontal portion of the Nusselt number curve is in close accord with the local steady-state Nusselt number for uniform wall temperature.

Convected energy flux

The performance of the duct as a heat exchanger will be characterized in terms of the energy carried out of the exit section by a given mass of fluid relative to that carried into the entrance section by the same fluid. Specifically, consider the mass of fluid passing into the duct during the "hot" part of the cycle, that is, when $(T - T_0) > 0$. In the course of its flow through the duct, this mass of fluid will exchange heat with the walls, with the result that it will carry out of the duct a different amount of energy from that with which it entered. Clearly, the smaller the energy flux at exit (relative to that at inlet), the more effective is the duct as a heat exchanger. A similar discussion pertains to the fluid which enters the duct during the "cold" part of the cycle.

Suppose that in some given cycle, the first element of hot fluid enters the duct at time t^* (which may be taken as zero without loss of generality). Then, taking note of equation (14), it is clear that the last element of hot fluid enters at time $t^* + \pi/\omega$. The enthalpy E_i carried into the duct by this mass of fluid is

$$E_i = \rho(2L)\,Uc_p \int_0^{\pi/\omega} (T - T_0)\,dt$$

$$= 4\rho c_p\, UL\,\Delta T_0/\omega \qquad (37)$$

where T_0 is taken as the datum state and $(T - T_0)$ is from equation (14).

If the exit section is located at a distance x from the duct inlet, then the aforementioned first and last elements of hot fluid respectively pass out of the duct at times $t^* + x/U$ and $t^* + \pi/\omega + x/U$. Correspondingly, the enthalpy E_x carried out of the duct is

$$E_x = \rho(2L)\, U c_p \int_{x/U}^{\pi/\omega + x/U} (T_b - T_0)\, \mathrm{d}t. \qquad (38)$$

The foregoing integral is evaluated in a straightforward manner by employing the temperature solution (15). The resulting expression is quite lengthy and is, therefore, omitted.

If consideration is given to fluid entering during the cold portion of the cycle, that is, when $(T - T_0) < 0$, the foregoing expressions for E_x and E_i continue to apply provided that multiplicative negative signs are affixed. For present purposes, the negative signs are of no consequence.

For the sake of comparison, the just-described energy quantities may also be evaluated by employing the quasi-steady solution. E_i remains unchanged, while the quantity $(T_b - T_0)$ appearing in equation (38) is now taken from equation (30). It was deemed desirable to obtain E_x results for two distinct interpretations of the quasi-steady model. The first (and more usual) approach is to assume that the heat-transfer coefficient is independent of x and is equal to the fully developed value. The second is to use local values of the heat-transfer coefficient. For both of these options, it still remains to decide which thermal boundary condition is to be used for generating the steady-state heat-transfer coefficients. On the basis of Figs. 5 and 6, the uniform wall temperature condition appears to be a reasonable choice. Correspondingly, the fully-developed and entrance region Nusselt numbers are given by

$$Nu = 2{\cdot}47,$$

$$Nu(x) = \left[\sum_{n=0}^{\infty} \exp(-\beta_n^2 \chi)\right] / \left[\sum_{n=0}^{\infty} \exp(-\beta_n^2 \chi)/\beta_n^2\right] \qquad (39)$$

where $\beta_n = (2n + 1)\,\pi/2$. These were employed in successively evaluating equations (30) and (38).

The results for the convective energy flux derived in the preceding paragraphs are presented in Figs. 7 and 8 in terms of the ratio E_x/E_i. This quantity is plotted as a function of the dimensionless axial distance χ for parametric values of b^*. The first of these figures shows results for the complete solution (solid lines) and for the quasi-steady model with Nu = constant (dashed lines). The second figure contains similar information, but the quasi-steady model is based on $Nu = Nu(x)$. In both figures, groups of curves are referred to either the upper or to the lower abscissa scale to avoid confusing overlap. The quantity a^* does not appear as a parameter in the figures, because the E_x/E_i results are independent of a^*. One encounters this finding when integrating equation (38). This outcome is plausible inasmuch as time lag effects due to the fluid heat capacity are accounted for in the integration limits of equation (38).

Consider first the general trends, setting aside until later the comparison between the complete and quasi-steady solutions. Within the range of the abscissa, it is seen that E_x/E_i decreases with increasing χ, indicating a general improvement of heat exchanger performance with increasing passage length. However, there are some interesting differences in detail depending on the value of b^*. At the larger b^*, good heat exchanger performance is already attained with relatively short passages, and only small gains are achieved by increases in passage length. On the other hand, when b^* is small, short passages are not very effective for exchanging heat between the hot and cold portions of the cycle.

A finding of practical interest is that, in the range of larger b^*, the results are relatively insensitive to b^*. The curves for $b^* = 10$ and 100 are coincident over a large part of the range, and the curve for $b^* = 5$ lies very close to these. Thus, the performance of the duct as a heat

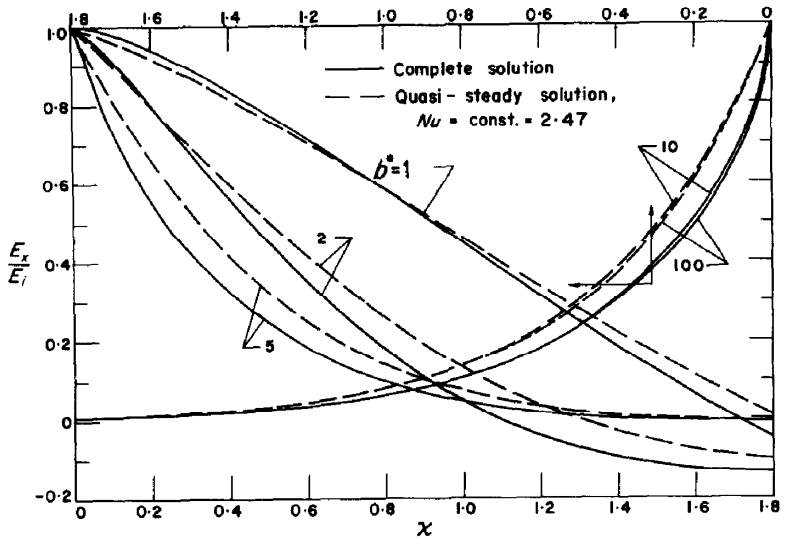

FIG. 7. Convected energy flux and comparison with quasi-steady solution for Nu = const. = 2·47.

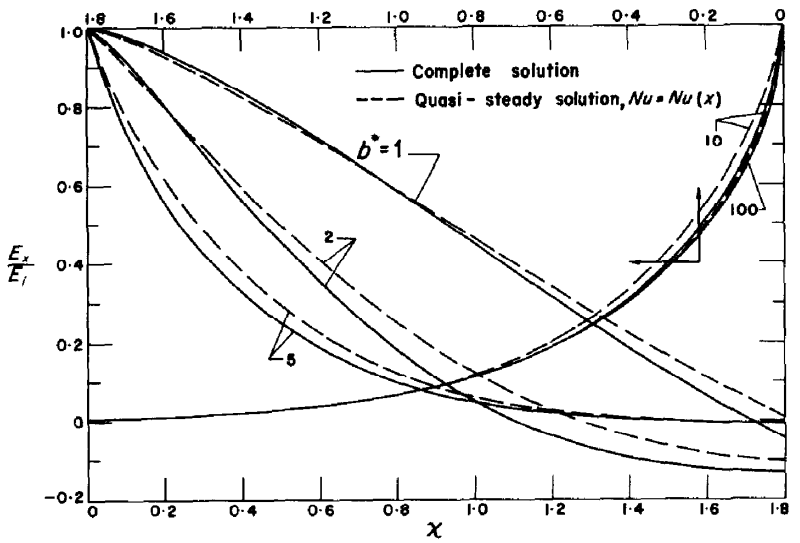

FIG. 8. Convected energy flux and comparison with quasi-steady solution for $Nu = Nu(x)$.

exchanger is described by a single curve in the practical range of b^*.

It can also be observed in Figs. 7 and 8 that E_x/E_i may take on negative values. This occurs because of the selection of T_0 as the datum for the enthalpy, and otherwise has no particular significance.

Finally, attention may be turned to the comparison between the complete solution, represented by equation (15), and the quasi-steady solution. Consider first the results from the quasi-steady model in which h is regarded as independent of x (Fig. 7, dashed lines), this approach being the most common one used in transient analyses of heat exchangers. Figure 7 shows that the quasi-steady results reproduce all

the trends exhibited by the complete solution. On the other hand, while gross errors are not incurred, the quantitative accuracy of the results from the quasi-steady model are only marginally satisfactory. The deviations may be ascribed to either or both of the following: (1) the heat-transfer process is not quasi-steady; (2) the heat-transfer process is not fully-developed. For the higher values of b^*, it is believed that the latter is the dominant factor, while at the lower b^*, both factors are important. One rather surprising aspect of Fig. 7 is the unexpectedly good agreement between the solid and dashed curves for $b^* = 1$.

Consider next the quasi-steady solution based on an x-dependent heat-transfer coefficient, for which results are shown in Fig. 8, dashed lines. From the figure, one sees that for $b^* = 100$ the quasi-steady results are in excellent accord with those from the complete solution, while the agreement for $b^* = 10$ is satisfactory. This is because, as demonstrated by Fig. 6, the heat-transfer process is nearly quasi-steady at high b^*. For the other b^* shown in Fig. 8, the agreement between the dashed and solid curves is somewhat better than that evidenced in Fig. 7, but deviations still exist.

On the basis of the foregoing, it may be concluded that for laminar duct flows, the quasi-steady model is a fruitful method of analysis at high b^*, but only when used in conjunction with local values of the heat-transfer coefficient.†

REFERENCES

1. W. M. KAYS and A. L. LONDON, *Compact Heat Exchangers*. McGraw-Hill, New York (1964).
2. M. JAKOB, *Heat Transfer*, Vol. II. Wiley, New York (1957).
3. M. PERLMUTTER and R. SIEGEL, Unsteady laminar flow in a duct with unsteady heat addition, *J. Heat Transfer* **83**, 432 (1961).
4. R. SIEGEL and M. PERLMUTTER, Laminar heat transfer in a channel with unsteady flow and wall heating varying with position and time, *J. Heat Transfer* **85**, 358 (1963).
5. J. L. HUDSON and S. G. BANKOFF, Asymptotic solutions for the unsteady Graetz problem, *Int. J. Heat Mass Transfer* **6**, 607 (1963).
6. A. KARDAS, On a problem in the theory of the unidirectional regenerator, *Int. J. Heat Mass Transfer* **9**, 567 (1966).
7. A. J. GRAM and G. W. KESSLER, New regenerative air heater, *Mech. Engng* **88**(9), 45 (1966).
8. B. FRIEDMAN, *Principles and Techniques of Applied Mathematics*. Wiley, New York (1962).
9. F. B. HILDEBRAND, *Advanced Calculus for Applications*. Prentice-Hall, Englewood Cliffs, New Jersey (1963).

† It was the opinion of one of the referees that the quasi-steady model with a constant Nu is a fruitful method of analysis provided that an average value for the interval 0 to x were employed in place of the fully-developed value.

APPENDIX

$$\Phi_n = \cos \gamma_n \eta \cosh \delta_n \eta$$

$$\varphi_n = \sin \gamma_n \eta \sinh \delta_n \eta$$

$$Z_n = F_n \cos \psi_n \chi - f_n \sin \psi_n \chi$$

$$\zeta_n = f_n \cos \psi_n \chi + F_n \sin \psi_n \chi$$

where

$$\psi_n = a^* b^* + 2\gamma_n \delta_n$$

$$F_n = \frac{t_n q_n - s_n r_n}{q_n^2 + r_n^2}$$

$$f_n = \frac{s_n q_n + t_n r_n}{q_n^2 + r_n^2}$$

and

$$q_n = 2\gamma_n + \sin 2\gamma_n \cosh 2\delta_n$$

$$r_n = 2\delta_n + \cos 2\gamma_n \sinh 2\delta_n$$

$$s_n = \sin \gamma_n \cosh \delta_n$$

$$t_n = \cos \gamma_n \sinh \delta_n.$$

Résumé—On a fait la théorie du transport de chaleur laminaire instationnaire dans un tuyau avec une température d'entrée variant périodiquement et des températures pariétales dépendant du temps et de l'espace. La variation de la température pariétale n'est pas spécifiée à l'avance, mais est plutôt déterminée par un bilan de la vitesse de transport de chaleur et de l'emmagasinement d'énergie. Dans la formulation théorique, l'hypothèse quasi-permanente employée habituellement est levée en faveur de l'application

locale de l'équation de l'énergie, dont la solution conduit à un problème de valeurs propres dans lequel ces valeurs propres sont complexes (parties réelles et imaginaires). Les propriétés des développements en série des fonctions propres complexes correspondantes, qui sont essentielles pour la solution, sont modifiées. Des résultats numériques sont obtenus pour la dépendance en fonction du temps et de l'espace des températures pariétale et globale et du nombre de Nusselt. Ces résultats sont identiques aux conditions sous lesquelles les variations de la température pariétale sont négligeables et le nombre de Nusselt instantané est virtuellement indépendant du temps. En outre, l'information numérique sur les performances globales du tuyau comme échangeur de chaleur est fournie au moyen du rapport du flux de chaleur de sortie au flux de chaleur d'entrée. On montre que dans une large gamme de conditions opératoires, les performances peuvent être décrites par une courbe unique. Dans un but de comparaison, les résultats pour les performances globales sont également obtenus en employant le modèle quasi-permanent. Les résultats quasi-permanents sont évalués pour des coefficients de transport de chaleur soit variables soit uniformes dans l'espace. On a trouvé que, dans une gamme de conditions opératoires, le modèle quasi-permanent est capable de donner des prévisions précises des performances, spécialement lorsqu'il est employé en liaison avec des coefficients de transport de chaleur variant dans l'espace.

Zusammenfassung—Der instationäre laminare Wärmeübergang in einem Kanal mit periodisch veränderlicher Einlasstemperatur und zeit- und orsabhängiger Wandtemperatur wurde analytisch untersucht. Die Festlegung der Wandtemperaturänderung erfolgt nicht im voraus, sondern dynamisch nach einer Bilanz des Wärmeübergangs und der Speicherenergie. In der analytischen Formulierung wird die gewöhnlich benützte quasi-stationäre Annahme aufgehoben, um die Energiegleichung örtlich anzuwenden, wobei die Lösung auf ein Eigenwertproblem führt mit komplexen (realen und imaginären Teilen) Eigenwerten. Die Eigenschaften der entwickelten Reihen der korrespondierenden komplexen Eigenfunktionen werden wegen ihrer Bedeutung für die Lösung variiert. Numerische Ergebnisse liessen sich erhalten für die zeit- und ortsabhängigen Temperaturen der Wand und des Mediums und für die Nusselt-Zahl. Diese Ergebnisse vermitteln die Bedingungen, unter welchen die Änderungen der Wandtemperatur vernachlässigbar sind und die augenblickliche Nusselt-Zahl im wesentlichen zeitabhängig ist. Ausserdem wird eine numerische Auswertung für das Gesamtverhalten des Kanals als Wärmeübertrager gegeben auf Grund des Verhältnisses von austretendem zu eintretendem Energiestrom. Es wird gezeigt, dass für einen grossen Arbeitsbereich das Gesamtverhalten durch eine einzige Kurve wiedergegeben werden kann. Zum Vergleich sind auch Ergebnisse für quasi-stationäres Verhalten mitgeteilt. Quasi-stationäre Ergebnisse wurden ermittelt, sowohl für räumlich gleichförmige wie auch veränderliche Wärmeübergangskoeffizienten. Es zeigte sich, dass für gewisse Arbeitsbereiche das quasi-stationäre Modell genaue Berechnungen erlaubt, besonders wenn es in Verbindung mit räumlich veränderlichen Wärmeübergangskoeffizienten verwendet wird.

Аннотация—Проведен анализ нестационарного ламинарного теплообмена в трубе с периодически изменяющейся температурой на входе и зависящей от времени и пространства температурой стенки. Изменение температуры стенки не задается заранее, а определяется динамически по балансу переноса и накопления энергии. В аналитической формулировке обычно используемые допущения квазистационарности заменены локальным применением уравнения энергии, решение которого приводит к проблеме характеристических значений, в которых характеристические значения являются комплексными (действительная и мнимая части). Свойства разложения в ряд соответствующих комплексных характеристических функций, которые являются важными для решения, изменялись. Получены численные значения чисел Нуссельта и временной и пространственной зависимости температур стенки и потока. Эти результаты определяют условия, при которых температурными изменениями стенки можно пренебречь, а мгновенное число Нуссельта фактичкски не зависит от времени. Кроме того, числовые данные по общей эффективности канала, служащей в качестве теплообменника, можно получить с помощью отношения выходящего потока энергии ко входящему. Показано, что для широкого диапазона рабочих условий общую эффективность можно представить одной кривой. Для сравнения результаты по общей эффективности получены также с использованием квази-стационарной модели. Эти данные вычислены с использованием как равномерных на отдельных интервалах, так и изменяющихся в пространстве коэффициентов теплообмена. Найдено, что для ряда рабочих условий квазистационарная модель может давать точные расчеты эффективности, особенно, когда она используется с коэффициентами теплообмена, изменяющимися в пространстве.